Recent Progress in Ultra-Wideband Microwave Breast Cancer Detection

Simone A. Winkler, Emily Porter, Adam Santorelli, Mark Coates, Milica Popović
Department of Electrical and Computer Engineering
McGill University
Montreal, QC, Canada
simone.winkler@mcgill.ca

Abstract—**This paper reports on progress in the field of breast cancer detection research carried out at McGill University. A low-cost time-domain system operating in the ultra-wideband (UWB) frequency range has been developed and successfully employed for early detection of breast tumors. Highly realistic breast phantoms with irregular shape and different tissue contents have been constructed specifically for the purpose of tumor detection. A new transmitter system using specific UWB pulse shaping has been introduced leading to improved tumor detection performance. Latest results are shown and presented in comparison to prior experiments.**

Keywords-breast cancer detection; microwave imaging; phantoms

I. Introduction

In 2011, an estimated 280,000 cases of breast cancer were diagnosed in the United States and Canada – with as many as 45,000 cases leading to death. For women, breast cancer mortality rates are higher than for any other cancer, with the exception of lung cancer [1], [2].

From these statistics, it is clear that it is of immediate and indisputable importance to find new methods for the early detection of breast cancer in order to provide treatment to patients as early as possible. This will not only reduce mortality and incidence rates, but also significantly ease the requirements on treatment and surgery, and the involved cost to the health care system.

Current breast cancer screening methods include mammography, ultrasound techniques, and magnetic resonance imaging (MRI). Mammography is the most common method currently being clinically employed and promoted as a regular screening method; however it suffers from a number of drawbacks: the patient's breast is required to undergo heavy compression in order to allow for the measurement, in addition it employs ionizing radiation and suffers from high false-positive and false-negative rates, which is not only very unpleasant for patients mentally and physically, but also represents a significant additional financial burden to health care systems, as it necessitates costly follow-up biopsies. Regarding alternate methods, ultrasound exams struggle with the distinction between malign and benign tumors, and MRI scans are highly expensive and complex.

Recent research suggests the use of microwaves for breast tumor detection, in particular the ultra-wideband (UWB) frequency region, offering a promising trade-off between imaging resolution and tissue penetration depth. The technique is based on the significant dielectric contrast between normal and cancerous breast tissues at microwave frequencies. Transmitting low-power microwave energy – in the form of UWB pulses – into the breast and receiving the backscattered field with a suitable antenna arrangement (radar-based approach) can be employed to create a 3-D image of the breast interior, making it possible to locate cancerous tissue with sub-cm resolution.

Currently, only a handful of research teams throughout the world are focusing their efforts on this topic [3], [4]. The parameter that distinguishes our system from other groups is its capability to measure in the time domain instead of the widely applied frequency domain systems. This method offers 1) a reduced acquisition time, and 2) much more cost-efficient equipment requirements.

The functionality of our system has been verified in a number of recent publications [5], [6]. The work progress on this topic has undergone a bottom-up approach from a more simplified study towards the measurement of complex scenarios in order to verify and perfect the technique for future in-vivo screening.

This paper represents an overview of the latest progress in our research, with major focus on the measurement of realistic breast models and improved transmission. Section II is concerned with the description of the breast phantoms constructed and measured in our research, and section III reports on the safety considerations that need to be met for employing the system for in-vivo screening. Section IV describes the system and measurement setup, while section V presents a selected overview of the most significant results obtained in the study.

II. Breast Phantoms

A major part of our ongoing research is concerned with the fabrication of realistic breast phantoms that allow us to verify the detection capacity of our system prior to in-vivo clinical testing. The materials in these phantoms have been designed to closely match the dielectric properties of human breast tissue [7] and have been empirically constructed from a variety of chemical materials, as shown in Table I.

TABLE I. LIST OF INGREDIENTS AND THE AMOUNT USED FOR EACH TISSUE PHANTOM

	Amount Used			
	Fat	***Skin***	***Gland***	***Tumor***
p-toluic acid (g)	0.133	0.294	0.253	0.346
n-propanol (mL)	6.96	28.69	12.71	17.00
deionized water (mL)	132.7	279.5	241.9	328.0
200 Bloom gelatin (g)	24.32	50.02	43.27	58.67
Formaldehyde (37% by weight) (g)	1.53	3.33	2.74	3.72
oil (mL)	265.6	98.6	141.5	38.4
Ultra Ivory detergent (mL)	12.00	5.86	6.79	2.00

The first series of phantoms were based on a hemispherical shape [7] in order to facilitate fabrication and post-processing for an initial feasibility study. As a part of this series, different types of tissue phantoms were made, ranging from simple fat-mimicking tissue, and phantoms including a thin skin layer, to highly realistic and more complex prototypes including gland content of different percentages. This bottom-up approach allowed us to gradually increase phantom complexity while maintaining system errors at a minimum. Table II shows the measured dielectric properties of the tissue mimicking materials [8] and the actual tissues [9] at 6 GHz. Also shown is the dielectric properties used in simulations, which have been matched to the tissue mimicking materials measurements using a best fit Debye model [8]. The variations in properties for the actual tissue measurements and the phantom measurements may seem significant, but tissue properties vary greatly and any difference seen here is within the expected range of actual tissue values. The exact data points for the excised tissue measurements from [9] were unavailable; those presented here have been estimated from plots.

TABLE II. DIELECTRIC PROPERTIES OF MODELED (EXPERIMENTAL AND SIMULATED) AND ACTUAL BREAST TISSUES AT 6 GHZ.

	Fat	***Skin***	***Gland***	***Tumor***
ε_r (phantom tissue measurement [8])	9.3	30	43	45
ε_r (actual tissue measurement [9])	4.5	35	42	48
ε_r (best fit Debye model [8])	9.5	31	44	46
σ (phantom tissue measurement [8]) (S/m)	1.4	5.1	3.9	6.9
σ (actual tissue measurement [9]) (S/m)	0.8	4.2	6.1	7.1
σ (best fit Debye model [8]) (S/m)	0.4	2.5	2.1	3.4

The current research step takes the hemispherical prototype a step further and makes use of realistically shaped breast phantoms. Fig. 1 shows a photograph of these phantoms, sized 17.5 x 16.5 x 8 cm^3. In particular, four different types were

Fig. 1 Photograph of a realistically shaped breast phantom (side and top view).

fabricated: a fat-only phantom with skin layer, and three phantoms adding 60%, 70%, and 80% glandular tissue, respectively. To mimic the interior of a real breast, the glands are conically shaped with the tip leading towards the nipple.

Breast tumors are also modeled to exhibit dielectrically appropriate properties and are cut into spherical shape with diameters of 0.5 cm, 1 cm, and 2 cm, respectively. The dimensions are based on the following assumptions: medical evidence suggests that in early stages of breast cancer tumors grow in spherical shape. Therefore, our system being aimed at early detection, this appears to be a viable scenario. The sizes selected here correspond to the dimensions of tumors in early stages, when detection is most beneficial for the patient's health and survival.

The tumors are inserted into the breast phantom by cutting an insertion slot. Also this appears to be realistic, as tumorous tissue tends to substitute healthy tissue instead of shifting and compressing it.

III. SAFETY CONSIDERATIONS

In the prospect of future in-vivo clinical trials, the safety of the system has been studied. The guidelines of the Health Canada Safety Code 6 [10] have been used for this study, with the guidelines for the United States and Europe imposing similar regulations. The code specifies limitations on the maximum level for the specific absorption rate (SAR). The time-averaged power density is calculated [10] as

$$W = \frac{1}{6} \sum_{i=1}^{n} W_i \, \Delta t_i \tag{1}$$

with W_i as the sampled power density in the i-th time period, i.e. the power density per pulse, and Δt_i is the duration of the i-th time period in minutes, i.e. the pulse duration in minutes; n corresponds to the number of pulses in a 6 minute period.

In our system with a repetition rate of 25 MHz or 40 ns, we transmit $9 \cdot 10^9$ pulses in a 6 minute period. The peak power per pulse is approximately 0.4 W based on a best-case estimated antenna efficiency of 50% (simulations give an average efficiency of 39%). These values yield a value for W in (1) of $7 \cdot 10^{-4}$ W. The calculated SAR for 1 g of tissue therefore calculates to a worst-case scenario of 0.7 W/kg. This value is well below both the limitations of 1.6 W/kg for uncontrolled environments and 8 W/kg for controlled environments (i.e. the patient being aware of exposure to fields and the associated risks, such as is the case in medical exams).

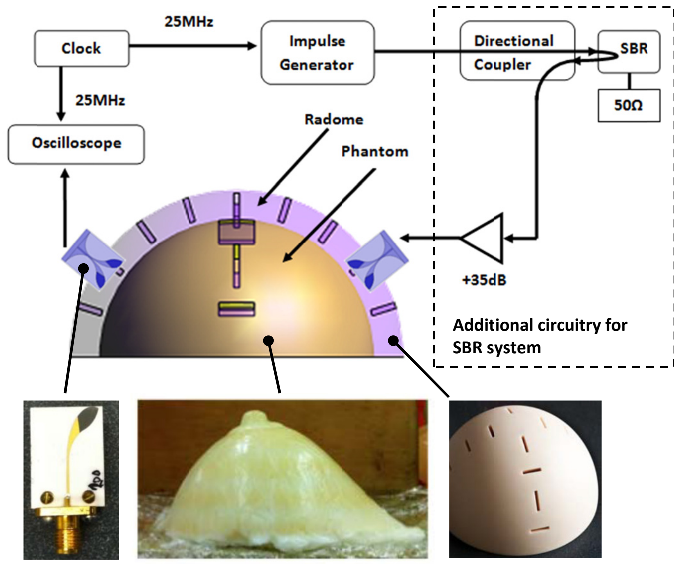

Fig. 2 Block diagram of early-detection system for breast cancer.

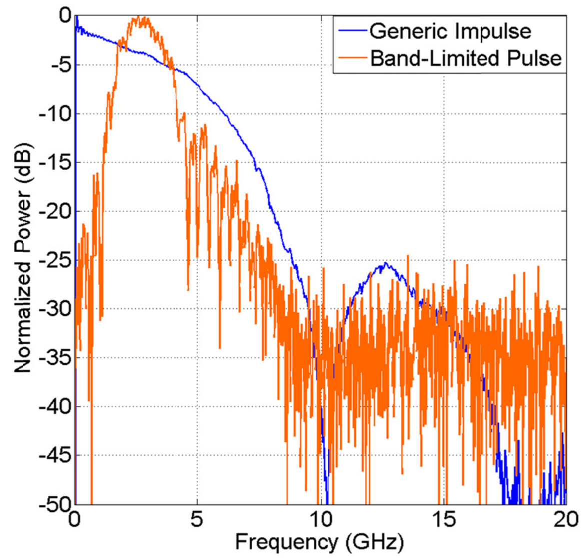

Fig. 3 Comparison of the spectra for the original pulse and the reshaped pulse used in the SBR system.

Additionally, the system has been approved by the McGill Research Ethics Board in conjunction with Health Canada as a safe environment for in-vivo clinical trials.

IV. Measurement System Setup

A. System overview

A block diagram of the system is shown in Fig. 2. A detailed description can be found in [5]. In summary, the system is based on a time-domain measurement and consists of a transmitting impulse generator, a hemispherical bowl-shaped radome used to hold both the breast phantom and the transceiver antennas, as well as the receiving circuitry collecting the signals with an oscilloscope. Transmitter/receiver paths are separated by a directional coupler. Two different transmission pulse schemes are used, as will be discussed in section IV.D. Considering the minimized number of components required in this system, it becomes now clear why a time-domain based measurement is of advantage in terms of system cost.

B. Antennas

The antennas employed here are Travelling Wave and Tapered Transmission Line Antennas as proposed in [11], selected for their large bandwidth and small size. Due to their endfire geometry, they are held in perpendicular slots on the exterior of the radome. The antennas work as transceivers, transmitting a pulse into the breast tissue and receiving the energy scattered off from tumors and/or other tissue discontinuities inside the breast.

C. Phantom placement

The breast phantom is inserted into the hemispherical radome. Its irregular shape and the consequent air gaps introducing significant signal losses require a fat-mimicking material serving as a matching medium between the radome walls and the breast phantom.

D. UWB pulse generation

A 70 ps pulse, triggered by a 25 MHz clock, is generated by an impulse generator and transmitted by the antenna. Two different pulses are used: 1) the original output from the pulse generator, and 2) a band-limited pulse proven to be more suitable for our purposes. In case the synthesized broadband reflector (SBR) pulse shaping technique is used, an additional 35 dB broadband amplifier is inserted to compensate for additional losses.

The pulse in 2) is shaped using a SBR in the form of a microstrip structure [12] and reshapes the spectral content as shown in Fig. 3. The frequency content of the pulse created from the impulse generator is not ideal for our experimental system as the majority of the power is in the low frequency range with decreasing power for higher frequencies.

Fig. 3 compares the spectral content of the generated impulse and the reshaped pulse employed in the SBR system. It demonstrates the ability of the SBR system to successfully reshape this generic impulse so that its main frequency content is contained in the 2-4 GHz range.

E. Receiving circuitry

An oscilloscope reads the data received by the antennas and records them as a time-domain signal.

V. Experimental Results

The measurements are carried out by first measuring a baseline signal for a healthy breast as a reference.[1] Then, a tumor is inserted into the phantom, and the measurement is repeated. The key metric for all results is presented as the tumor response, i.e. the difference between the received

[1] This baseline signal is for experimental use only, in order to prove principal functionality. A future system will not use this baseline measurement and will instead use detection algorithms.

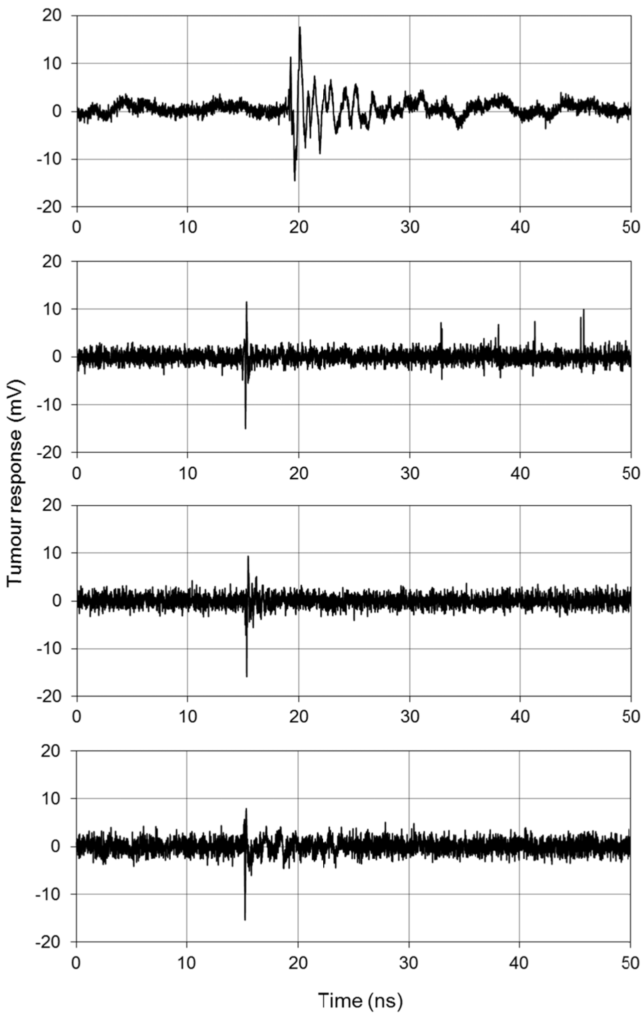

Fig. 4 Comparison of scattered signal for breast phantoms with no gland content, as well as 60%, 70%, and 80% of gland content, respectively (all cases use a tumor size of 1 cm).

backscatter signal with a tumor present and the healthy baseline signal.

The tumors for all measurements are located at a depth of approximately 1 cm from the chest wall vertically, as well as halfway between the radome wall and the radome center horizontally.

The measurements are exclusively shown for the case of co-polarized antennas used in two immediately adjacent slots. This configuration has proven the most useful for assessing the backscatter from tumors [5], as it provides the quasi-direct reflection path for the transmitted signal. The signals for all other receiving antennas are recorded as well but are not included in this discussion. They are used in 3-D image processing algorithms and therefore less significant for the presented work focusing on time-domain backscatter results.

In each of the experiments, the antennas are located in the stack of slots centered between the chest wall and the halfway-point of chest and nipple. For sake of consistency, this scenario is denoted as 'case 5' with referral to past work.

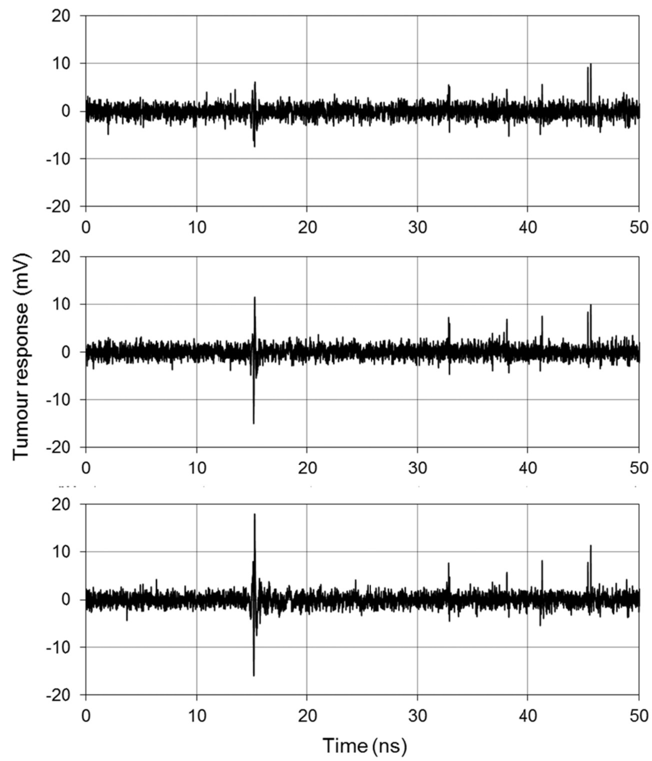

Fig. 5 Comparison of scattered signal for breast phantoms with small (0.5 cm), medium (1 cm), and large (2 cm), respectively (all cases use a gland content of 60%).

In the following graphs, for each case, one period of the recorded signal is presented. No manual averaging of data is performed. The graphs show the tumor response signal in millivolts in order to get insight into the pulse waveform of the reflected signals.

Fig. 4 presents a comparison of backscatter signals for each of the different breast phantoms constructed, as described in section II. The results are presented for a phantom with skin and fat only, and for the three phantoms with 60%, 70%, and 80% of gland content, respectively. Each of the cases was tested with a tumor with a size of 1 cm. The offset in time is not to be considered, as it only arises from different phase delays in different measurement setups.

From the results in Fig. 4, we can see that in each of the phantoms, the tumor is successfully detected. We also note that the clutter increases as the gland percentage increases. This is due to the fact that tumors and glands exhibit very similar dielectric properties. The presented results thus represent a very good result proving that a tumor can be detected even in a highly glandular breast tissue, being the most difficult scenario.

A further interesting result is the variation in tumor response for different tumor sizes as shown in Fig. 5. This result is shown for a breast phantom with 60% gland content. It is clearly visible that the tumor response increases with larger tumor size. Even the smallest tumor is easily detected with the tumor response lying well above the noise floor.

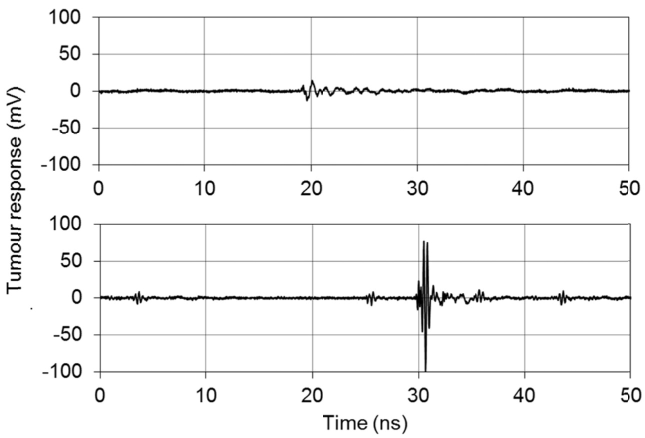

Fig. 6 Comparison of scattered signal for the non-SBR and the SBR system using a skin+fat phantom (both cases use a tumor size of 0.5 cm).

Finally, the performance between the SBR system as described in section IV.D and the original non-SBR system is presented in Fig. 6. Again, the time reference is not to be considered, as different phase delays occur for different transmitter systems. Also, the differences in signal amplitudes serve only as an approximate guideline, as the input transmitting signals are slightly different (non-SBR system: 6.3 V, SBR system: 7.8 V); they however still validate that the tumor response for the SBR system is greatly increased and is now symmetric and compact. Furthermore, the SBR response does not include any low-frequency response, thus eliminating the ringing tail of the non-SBR system. The additional reflections visible in Fig. 5b are attributed to additional reflections due to matching imperfections in the connections of the measurement system.

TABLE III. EXPERIMENTAL RESULTS FOR THE FOUR PRESENTED BREAST PHANTOMS (TUMOR SIZES: S = 0.5 CM, M = 1 CM, L = 2 CM, N/A: NOT MEASURED CASES)

Tumor size		***Skin+Fat***	***Skin+Fat +60% Gland***	***Skin+Fat +70% Gland***	***Skin+Fat +80% Gland***	***Skin+Fat (SBR System)***
S	mV	14.82	9.94	5.25	14.81	38.63
	dB	-52.6	-56.1	-61.63	-52.63	-46.08
M	mV	17.65	15.00	7.88	15.37	100.80
	dB	-51.1	-52.5	-58.11	-52.30	-37.75
L	mV	n/a	17.88	15.81	13.13	n/a
	dB	n/a	-51.0	-52.06	-53.67	n/a

In addition, Table III shows each of the results as the maximum tumor response in millivolts. In order to allow for a better comparison of the results, especially in the case of the non-SBR and the SBR system where transmit levels are slightly different due to the modified transmitter architecture, a relative measurement is introduced. The relative tumor response is defined as the ratio of maximum tumor response to the input level and is given in dB.

VI. CONCLUSIONS

The work presented in this paper compares results for UWB time-domain early breast cancer detection in realistic irregularly-shaped breast phantoms. We show that for the newly developed phantoms with varying percentage of glandular tissue, a tumor of different size can be detected successfully. We also present a new transmitter structure employing a shaped pulse adapted to the requirements of breast cancer detection. This system is denoted as the SBR system in the paper. The results for the latter, in comparison with the original system, exhibit vastly improved tumor detection capability and signal shape. In addition, we report on the safety of our system in terms of microwave radiation characteristics.

REFERENCES

[1] Canadian Cancer Society, "Canadian Cancer Statistics 2010", Online publication. Available: http://www.cancer.ca

[2] Breastcancer.org "U.S. Breast Cancer Statistics 2010", Online publication. Available: http://www.breastcancer.org/

[3] E. C. Fear et al., "Experimental feasibility study of confocal microwave imaging for breast tumor detection," *IEEE Trans. Microw. Theory Tech.*, vol. 51, Iss. 3, pp. 887–892, March 2003.

[4] M. Klemm et al., "Radar-Based Breast Cancer Detection Using a Hemispherical Antenna Array – Experimental Results", *IEEE Trans. Ant. Prop.,* vol. 57, Iss. 6, pp. 1692–1704, June 2009.

[5] E. Porter et al., "An Experimental System for Time-Domain Microwave Breast Imaging", *Proc. European Conf. Antennas Propag.*, Rome, Italy, pp. 2906–2910, Apr. 2011.

[6] E. Porter, A. Santorelli, S. Winkler, M. Popovic, M. Coates, "Time-Domain Microwave Cancer Screening: Optimized Pulse Shaping Applied to Realistically Shaped Breast Phantoms," *Proc. Int. Microw. Symp.*, Montreal, Canada, Jun. 2012.

[7] E. Porter et al., "Improved Tissue Phantoms for Experimental Validation of Microwave Breast Cancer Detection", *Proc. European Conf. Antennas Propag.*, Barcelona, Spain, pp. 1–5, Apr. 2010.

[8] A. Santorelli, "Breast screening with custom-shaped pulsed microwaves (ch. 4)," *Master's thesis,* McGill University, Montreal, 2012.

[9] M. Lazebnik et al., "A large-scale study of the ultrawideband microwave dielectric properties of normal, benign and malignant breast tissues obtained from cancer surgeries," *Phys. Med. Biol.*, vol. 52, pp. 6093–6115, 2007.

[10] Health Canada, "Limits of Human Exposure to Radiofrequency Electromagnetic Energy in the Frequency Range from 3 kHz to 300 GHz –Safety Code 6", Ottawa, 2009.

[11] H. Kanj, "Resistively-loaded antenna designs for ultra-wideband confocal microwave imaging of breast cancer," *Ph.D. Thesis*, McGill University, Aug. 2007.

[12] I. Arnedo; J.D. Schwartz; M.A.G. Laso; T. Lopetegi; D.V. Plant; J. Azaa;, "Passive microwave planar circuits for arbitrary UWB pulse shaping," *IEEE Microw. Wireless Comp. Lett.*, vol.18, Iss.7, pp. 452–454, July 2008.